INTERNATIONAL JOURNAL FOR NUMERICAL METHODS IN FLUIDS
Int. J. Numer. Meth. Fluids 2001; **37**: 149–174 (DOI: 10.1002/fld.168)

Spectral analysis of flux vector splitting finite volume methods

Tapan K. Sengupta[a,*], D. Sridar[a], S. Sarkar[b] and S. De[b]

[a] *Department of Aerospace Engineering, Indian Institute of Technology, Kanpur, India*
[b] *Department of Mechanical Engineering, Indian Institute of Technology, Kanpur, India*

SUMMARY

New results are presented here for finite volume (FV) methods that use flux vector splitting (FVS) along with higher-order reconstruction schemes. Apart from spectral accuracy of the resultant methods, the numerical stability is investigated which restricts the allowable time step or the Courant–Friedrich–Lewy (CFL) number. Also the dispersion relation preservation (DRP) property of various spatial and temporal discretization schemes is investigated. The DRP property simultaneously fixes space and time steps. This aspect of numerical schemes is important for simulation of high-Reynolds number flows, compressible flows with shock(s) and computational aero-acoustics. It is shown here that for direct numerical simulation applications, the DRP property is more restrictive than stability criteria. Copyright © 2001 John Wiley & Sons, Ltd.

KEY WORDS: finite volume methods; flux vector splitting; spectral analysis

1. INTRODUCTION

For incompressible flows, spectral analyses of different spatial and temporal finite difference discretizations have been reported in References [1–3]. Apart from showing the spectral accuracy of different schemes, the dispersion relation preservation (DRP) property of these schemes showed that higher-order schemes have the potential to be used for direct numerical simulation (DNS) and large-eddy simulation (LES) with available computers. In the continuing investigation here, finite volume (FV) methods that use flux vector splitting (FVS) are investigated—including some higher-order spatial reconstruction and higher-order multi-step time integration schemes. As in Sengupta and Gupta [2], the DRP property is also quantified by looking at the numerical group velocity in comparison to the actual group velocity. For a

* E-mail: tksen@iitk.ac.in

Received July 1999
Revised February 2000

general space and time dependent problem, the group velocity is an indicator of energy propagation speed of the fluid dynamical system. Here, a 5 per cent deviation between the two is used as the acceptable limit for dispersion error. In general any discrete computation method, other than the spectral method, suffers phase error and this error is a measure of the spurious numerical dispersion as opposed to the actual physical dispersion. In addition there are other sources of errors that affect numerical computations. For example, at high Reynolds numbers the aliasing error can cause serious problems to high spectrally accurate schemes [4], while it is not important for low-order schemes. For higher-order upwind schemes the built-in numerical dissipation partially offsets this problem and for the same reason in spectral methods numerical dissipation is often added and is known as *hypervis-cosity* [2]. The role of numerical dissipation of higher-order upwind schemes in providing *sub-grid scale* (SGS) stresses for LES is established in Sengupta and Nair [3]. Furthermore, it can be shown that in discrete computation the evaluation of physical dissipation in the physical plane is deficient while in the transformed plane it is a serious source of aliasing error.

In References [5,2] some preliminary analyses have been reported for the FVS-FV methods for compressible flows. In this research the same is extended to investigate stability and the dispersion property of some of the traditional methods as well as a new scheme that uses a slope limiter [6] to control non-linear numerical instability for spatial discretization. Additionally, various time-integration schemes that are used for DNS and LES, namely the Adams–Bashforth and multistage Runge–Kutta schemes are also investigated.

In the next section the analyses of such discrete schemes as applied to a model wave equation are demonstrated. The adoption of a wave equation allows direct investigation of dispersion phenomena and the associated DRP property. In many fluid dynamic systems, governed by either elliptic or hyperbolic partial differential equations or a mixed elliptic-hyperbolic system, the wave nature of the disturbance field is important and hence an examination of the wave equation *vis-à-vis* its solution by different numerical strategies is in order. While the wave equation is non-dispersive, it is important to calibrate numerical methods for allowable wave numbers and circular frequency ranges for the space and time steps for which the numerical scheme is used. The results of this analysis are interpreted in the sense that if a scheme is unsuitable for solving a non-dispersive wave equation, it will be equally unsuitable for a general dispersive fluid dynamic system governed by either Euler or Navier–Stokes equations. The final section contains the results and discussion, which provides guidelines about numerical schemes.

2. ANALYSES OF FVS-FV METHODS

Consider a one-dimensional wave equation that admits disturbances propagating from left to right at a constant phase speed c

$$\frac{\partial u}{\partial t} + c\frac{\partial u}{\partial x} = 0 \tag{1}$$

It should be noted that for the above system, the finite group of waves also transmits its energy at the same velocity, i.e. the group velocity V_g of Equation (1) given by

$$V_g = c \tag{2}$$

To allow for spectral analyses consider discretization on a uniform grid of size Δx and Δt, in space and time respectively. Since disturbances only propagate in the positive x-direction, the discrete FV version of Equation (1) is given for the lth cell

$$\frac{U_l^{n+1} - U_l^n}{\Delta t}\,\Delta x + c(U^+_{l+1/2} - U^+_{l-1/2}) = 0 \tag{3}$$

The second set of terms in Equation (3) represents the balance of outgoing fluxes and incoming fluxes through the cell interfaces.

2.1. FVS schemes

The flux terms $U^+_{l\pm 1/2}$ on the cell interfaces can be reconstructed by a class of interpolation schemes described in Hirsch [7] as

$$U^+_{l-1/2} = U_{l-1} + \frac{\varepsilon}{4}[(1-\kappa)(U_{l-1} - U_{l-2}) + (1+\kappa)(U_l - U_{l-1})]$$

$$U^+_{l+1/2} = U_l + \frac{\varepsilon}{4}[(1-\kappa)(U_l - U_{l-1}) + (1+\kappa)(U_{l+1} - U_l)] \tag{4}$$

When $\varepsilon = 0$, one recovers the first-order upwinding schemes and for $\varepsilon = 1$ one gets different higher-order schemes depending on the value of κ as

(a) $\kappa = -1$ gives a one-sided-linear (OSL) interpolation scheme.
(b) $\kappa = 0$ gives a linear interpolation (LI) scheme.
(c) $\kappa = 1$ is for a second-order accurate central difference (CD_2) scheme.
(d) $\kappa = \frac{1}{2}$ is for a QUICK scheme—a third-order accurate scheme.
(e) $\kappa = \frac{1}{3}$ is for a montone upstream-centered scheme for conservation laws (MUSCL)—another third-order accurate scheme.

Furthermore, if one represents the unknown U_l at the lth cell, by its bilateral Fourier–Laplace transform as

$$U(x_l, t) = \iint \hat{U}(k, \omega)\, e^{i(kx - \omega t)}\, dk\, d\omega \tag{5}$$

Then using Equations (5) and (4) in Equation (3) yields the following relation:

$$\frac{e^{-i\omega t}-1}{\Delta t}\Delta x + c\left\{(e^{-ik\Delta x}-1)+\frac{\varepsilon(1-\kappa)}{4}[2e^{-tk\Delta x}-1-e^{-2ik\Delta x}]\right.$$
$$\left.+\frac{\varepsilon(1+\kappa)}{4}[2-e^{-ik\Delta x}-e^{ik\Delta x}]\right\}=0 \tag{6}$$

The above (ε–κ) class of schemes gives rise to the following amplification factor:

$$G(k)=G_{\text{real}}+iG_{\text{imag}} \tag{7}$$

where

$$G(k)=\frac{\tilde{U}(k,t+\Delta t)}{\tilde{U}(k,t)}$$

is $\tilde{U}(k,t)$ the Laplace transform of $U(x,t)$. In general, $G(k)$ will be a complex quantity and for the scheme given by Equation (4)

$$G_{\text{real}}=1-2N_C\sin^2\left(\frac{k\Delta x}{2}\right)\left[1-\varepsilon\left(\cos^2\frac{k\Delta x}{2}+\kappa\sin^2\frac{k\Delta x}{2}\right)\right]$$

$$G_{\text{imag}}=-N_C\sin(k\Delta x)\left[1+\varepsilon(1-\kappa)\sin^2\frac{k\Delta x}{2}\right]$$

where

$$N_C=\frac{c\Delta t}{\Delta x}$$

is the Courant–Friedrich–Lewy (CFL) number.

From Equation (6) one can also write down the dispersion relation of the discrete scheme as

$$\sin(\omega\Delta t)=N_C\sin(k\Delta x)\left[1+\varepsilon(1-\kappa)\sin^2\frac{k\Delta x}{2}\right] \tag{8}$$

From Equation (8) the numerical group velocity (V_{gn}) is obtained as

$$V_{\text{gn}}=\frac{d\omega}{dk}=\frac{c}{\cos(\omega\Delta t)}\left\{\cos(k\Delta x)\left[1+\varepsilon(1-\kappa)\sin^2\frac{k\Delta x}{2}\right]+\frac{\varepsilon(1-\kappa)}{2}\sin^2\frac{k\Delta x}{2}\right\} \tag{9}$$

The above analysis estimates the amplification factor (G) and numerical group velocity when time is discretized by the Euler scheme, while the space discretization is obtained via Equation (4). If one wants to perform the dispersion analysis in semi-discrete from, i.e. when time is not discretized, then the corresponding dispersion relation can be obtained once again from Equation (8) by looking at the time continuum limit of ($\omega\Delta t\to 0$) and thus replacing the left

hand side by $\omega\Delta t$. Thus, the corresponding expression for the semi-discrete group velocity is obtained from Equation (9) by replacing $\cos(\omega\Delta t)$ by one in the denominator.

2.2. Slope limiter scheme

This method is adopted in Causon *et al.* [6], for developing high-resolution shock capturing scheme for transient analysis. The piecewise interpolation for reconstruction requires maintaining the positivity by eliminating non-physical oscillation. This is achieved by limiting the slope of the variable locally. The detailed steps are given by the following:

(i) In each cell the gradient (g_1) of the variable is computed by a second-order accurate discretization at the cell center.
(ii) At the cell interface, limit the unknown by using g_1 in the following manner

$$U_{l+1/2} \approx U_l + \alpha g_l \frac{\Delta x}{2} \leq \max(U_l, U_{l+1}) \geq \min(U_l, U_{l+1})$$

and

$$U_{l+1/2} \approx U_l - \alpha g_l \frac{\Delta x}{2} \leq \max(U_l, U_{l-1}) \geq \min(U_l, U_{l-1}) \tag{10}$$

α is maximized subject to

(a) $0 \leq \alpha \leq 1$
(b) $U_{l\pm1/2}$ in Equation (10) does not cause under- or overshoots at the cell interfaces. If U_{l_1} and U_{r_1} are the left and right running disturbance quantity at the $(l-\frac{1}{2})$ cell interface and U_{l_2} and U_{r_2} are the corresponding quantity at the $(l+\frac{1}{2})$ cell interface, then

$$U_{l_1} - U_{r_1} = (\alpha - 1)\Delta x U_l' - (\alpha - 1)\frac{\Delta x^2}{2} U_l''$$

$$U_{l_2} - U_{r_2} = (\alpha - 1)\Delta x U_l' + (\alpha - 1)\frac{\Delta x^2}{2} U_l'' \tag{11}$$

The prime indicates a derivative with respect to x in Equation (11). This scheme prevents formation of any new maximum and minimum at the cell interface by limiting the slope and thus this is truly a total variation diminishing (TVD) scheme. Also note that despite the claim of this scheme to be a high accuracy scheme, the cell interface fluxes are zeroth-order accurate if one chooses a constant α—as is evident from Equation (11). Using the cell interface values of the unknown in Equation (3), one can obtain the real and imaginary component of the amplification rate as

$$G_{\text{real}} = 1 - 2N_{\text{C}} \sin^2 \frac{k\Delta x}{2}\left[1 - \alpha \cos^2 \frac{k\Delta x}{2}\right]$$
$$G_{\text{imag}} = -N_{\text{C}} \sin(k\Delta x)\left[1 + \frac{\alpha}{2}(1 - \cos(k\Delta x))\right] \tag{12}$$

The corresponding numerical group velocity is given by

$$V_{\text{gn}} = \frac{c}{\cos(\omega\Delta t)}\left\{\cos(k\Delta x) - \frac{\alpha}{2}\cos(k\Delta x) + \frac{\alpha}{2}\cos(2k\Delta x)\right\} \tag{13}$$

3. RESULTS AND DISCUSSION

The amplification factor, $G(k)$, for the FVS schemes as given by Equation (7) and is plotted in Figure 1 for $N_{\text{C}} = 0.1$. Excepting the second-order central difference scheme, all the other schemes show numerical stability. It is worth recalling that the physical situation depicted by Equation (1) is actually neutrally stable. Thus, to represent such a situation, one must adopt a numerical scheme that is as close to neutral stability as possible. As the CFL number is reduced, all the schemes show a move towards the right direction and it is only the central difference scheme that approaches neutral stability from the unstable side and hence cannot be used for even solving the one-dimensional wave equation. For the other schemes given by Equation (7), different schemes perform differently depending on the amount of numerical dissipation that is implicit with the upwinding. For example, one-sided linear interpolation and first-order upwind schemes are the most dissipative at all wave numbers in the range of interest ($0 \leq k\Delta x \leq \pi$). Next in the order of added dissipation is the linear interpolation scheme. Between the two higher-order upwind schemes, MUSCL adds more dissipation as compared to QUICK.

The region where numerical group velocity matches with the physical group velocity within ± 5 per cent tolerance is designated as the DRP region and, for the (ε–κ) schemes given by Equation (7), is plotted in Figure 2. The second-order accurate central difference scheme and first-order upwind scheme have identical phase relations, and thus show identical DRP regions. It should be pointed out that the region diagonally opposite to the origin shows a patch of DRP region where the numerical group velocity is close to the actual group velocity. This can be understood by looking at the expression given by Equation (9). For example, for the second-order central difference scheme the expression for numerical group velocity can be simplified to

$$V_{\text{gn}} = c\,\frac{\cos(k\Delta x)}{\cos(\omega\Delta t)} \tag{13a}$$

Thus, although locally the phase error is maximum, for these combinations of wave numbers and circular frequencies, the dispersion error as given by the numerical group velocity is minimum and given by a ratio of symmetric functions. Thus, it is apparent that the patch close to the origin is of interest for the least dispersion error. From this point of view, it is the QUICK and MUSCL schemes that are seen to be ideal for high accuracy FVS-FV computing,

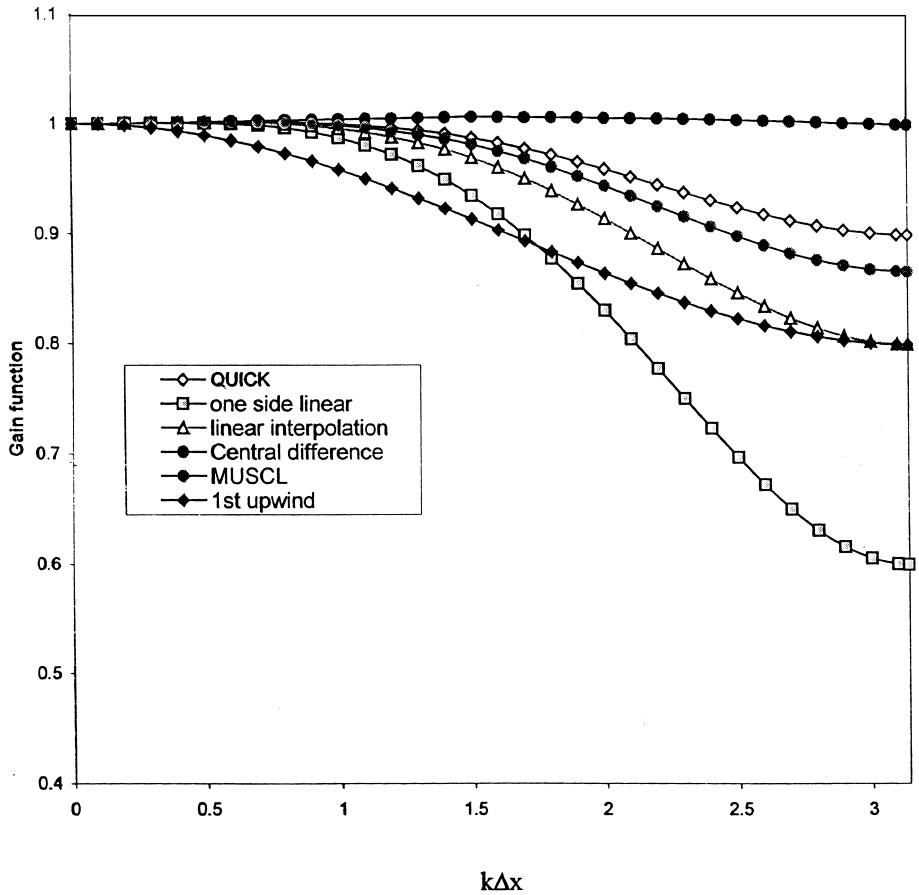

Figure 1. The amplification factor (G) for (ε–κ) flux vector splitting FV schemes for which time integration is performed by the Euler method for the wave equation, plotted against possible non-dimensional wave numbers ($0 \leq k\Delta x \leq \pi$).

with MUSCL having a larger range of wave numbers where the DRP property is better. All the schemes show the same circular frequency ranges because of the same time integration scheme used for all the discretization schemes. Also, note that the results of semi-discrete analysis—where time is not discretized—can be directly noted from these figures by looking at them for $\omega\Delta t \to 0$ and from this point of view the MUSCL and linear interpolation schemes also show the maximum promise.

In Figure 3, the amplification factor $G(k)$, of the slope limiter scheme as given by Equation (12), is shown for different CFL numbers for $\alpha = 0.1$ and 0.5. In the actual applications the value of α is maximized for the slope, such that the unknowns at the cell interface do not exceed or fall below the neighboring cell-center values of the unknown. In this context the

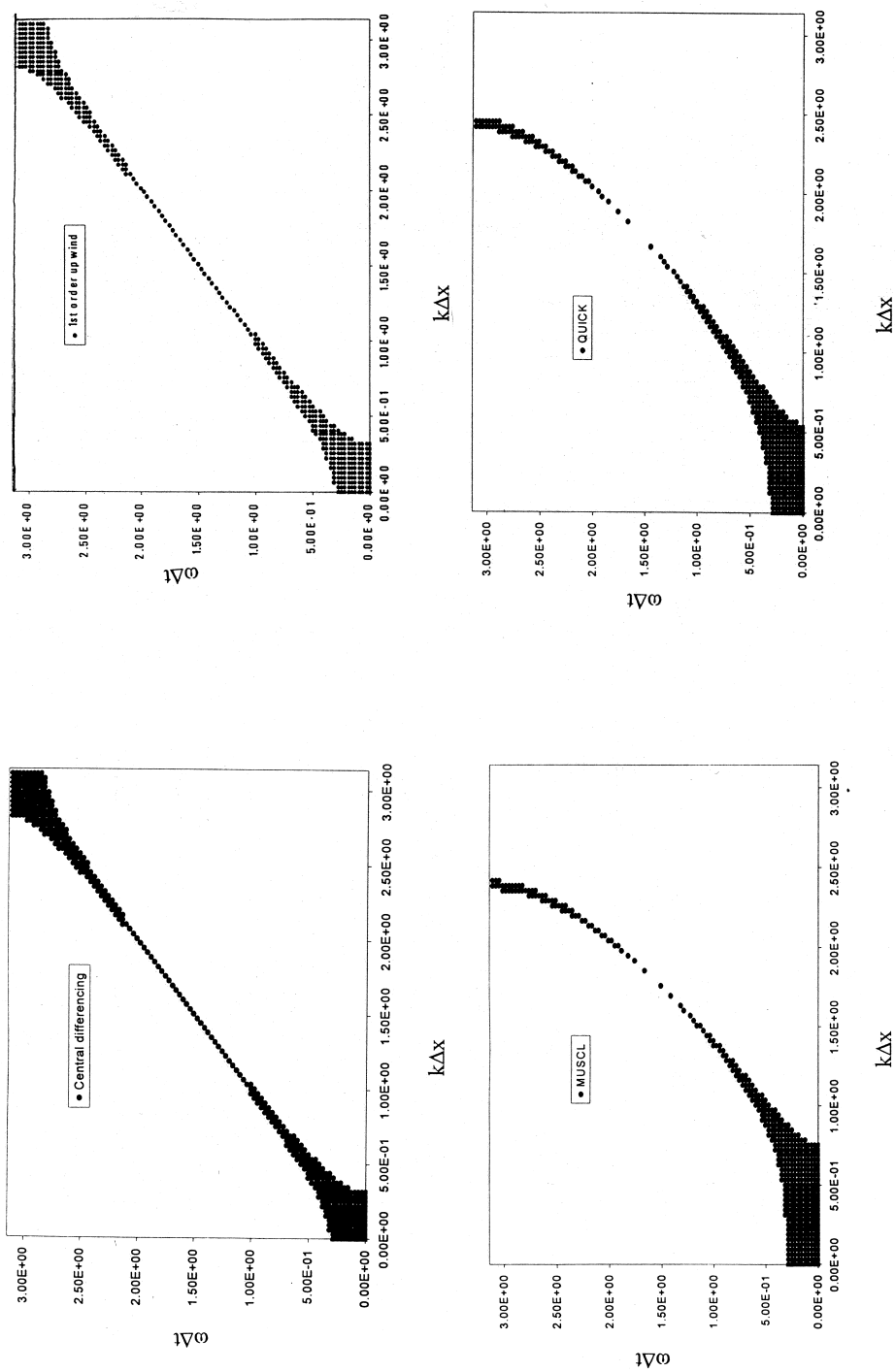

Figure 2. DRP region in non-dimensional wave number-frequency plane for different flux vector reconstruction schemes: (a) CD_2; (b) first-order upwinding; (c) MUSCL; and (d) QUICK.

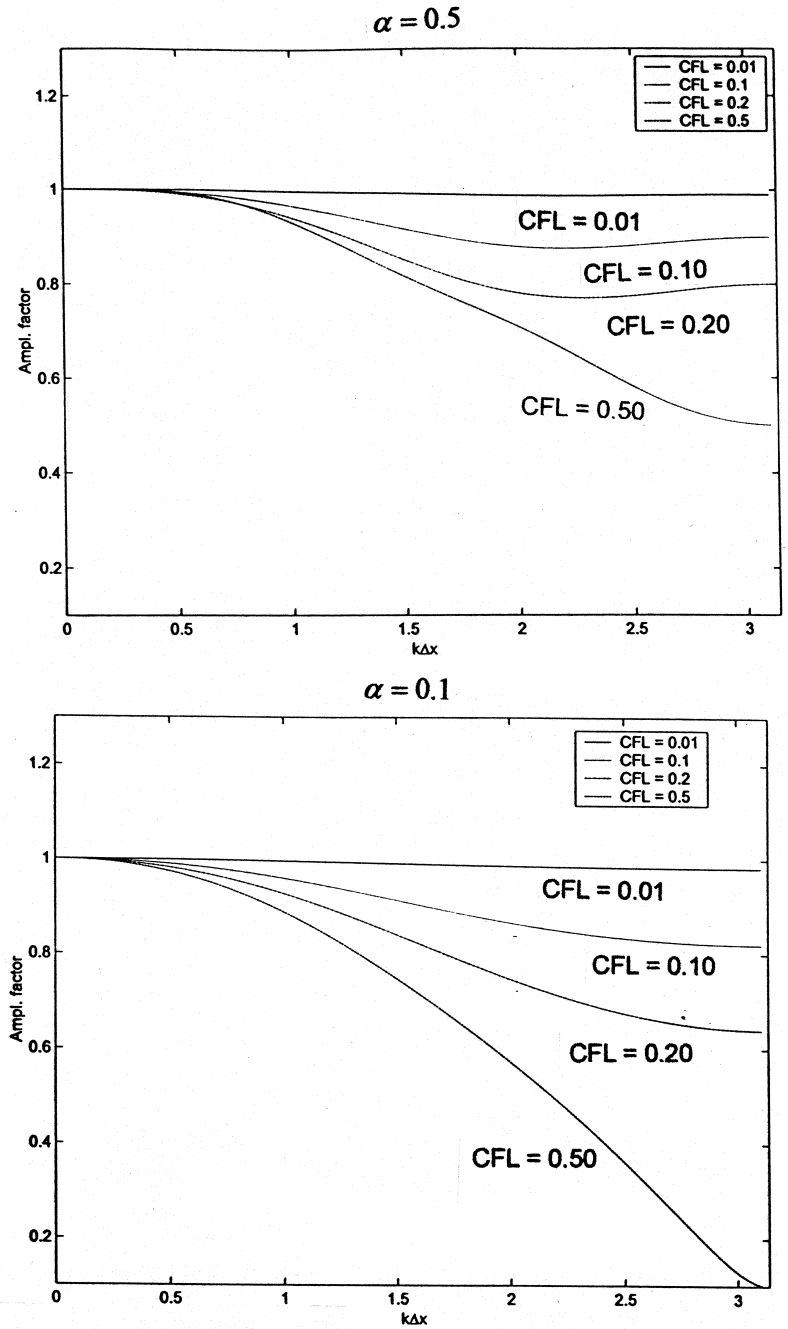

Figure 3. The amplification factor (G) for the slope limiter scheme [6] plotted against non-dimensional wave numbers. Shown are results for two values of the limited slopes.

above value of α is chosen as arbitrary. This is a non-linear limiter scheme and this fact is amply demonstrated in Figure 3. Among all the three values of CFL number for $\alpha = 0.5$, the highest CFL number exhibits excessive dissipation. The plotted figure clearly establishes the need to choose CFL numbers as small as possible. This is also the conclusion one draws for the FVS schemes shown in Figure 1. The figure for $\alpha = 0.1$ simply demonstrates that for the same CFL numbers the dissipations added are large and it is mandatory to choose very small value CFL numbers for higher accuracy.

DRP plots for the slope limiter scheme are displayed in Figure 4 for the same values of the limited slopes ($\alpha = 0.1$ and 0.5). It is seen that the DRP property degrades when α increases. The continuous region near the origin in the $(k\Delta x - \omega\Delta t)$ plane is really the area of interest that would give the wave number and circular frequency range, where DNS would be possible for physical systems governed by hyperbolic PDE or elliptic problems with wave-like solutions. This scheme was developed with the idea of accurate simulation of unsteady problems and for many fluid dynamic systems such unsteadiness is dominated by wavy evolution of flow variables.

The fact that the amplification factors, given by Equation (7), suggests that the CFL number will be severely restricted by all the single step methods, prompts one to look at the multi-step time integration schemes. In this context higher-order time stepping schemes are worth investigating for compressible flows—as was investigated in Sengupta and Gupta [2] for incompressible flows. If one uses the same spatial discretization scheme for the FVS scheme—the (ε–κ)—then one can start with Equation (1) and apply the second-order Adams–Bashforth time integration scheme given by

$$U_l^{n+1} = U_l^n + \frac{\Delta t}{2}\left[3\left.\frac{\partial u}{\partial t}\right|_l^n - \left.\frac{\partial u}{\partial t}\right|_l^{n-1}\right]$$

The equivalent of Equation (3) will be given by

$$U_l^{n+1} = U_l^n - \frac{N_C}{2}\left[3U_{l+1/2}^{n^+} - 3U_{l-1/2}^{n^+} - U_{l+1/2}^{n-1^+} + U_{l-1/2}^{n-1^*}\right] \tag{14}$$

Once again using the cell-face quantities, as given by Equation (4), one gets the computational molecule. The use of Fourier representation, given by Equation (5), in this computational molecule gives the numerical dispersion relation

$$\begin{aligned}\sin(\omega\Delta t) = {} & \frac{N_C}{2}\sin(k\Delta x)\left\{\frac{3\varepsilon}{2} + 3 - \frac{3\varepsilon}{4}\left[(1-\kappa)(2\cos(k\Delta x) - 1) + 1 + \kappa\right]\right\} \\ & + \frac{N_C}{2}\cos(\omega\Delta t)\sin(k\Delta x)\left\{\frac{\varepsilon}{2} + 1 - \frac{\varepsilon}{4}\left[(1-\kappa)(2\cos(k\Delta x) - 1) + 1 + \kappa\right]\right\} \\ & - \sin(\omega\Delta t)\left\{\left(1 - \frac{\varepsilon}{2}\kappa\right)(1 - \cos(k\Delta x))\right. \\ & \left. - \frac{\varepsilon}{4}\left[1 + \kappa - 2\kappa\cos(k\Delta x) - (1-\kappa)\cos(2k\Delta x)\right]\right\}\end{aligned} \tag{15}$$

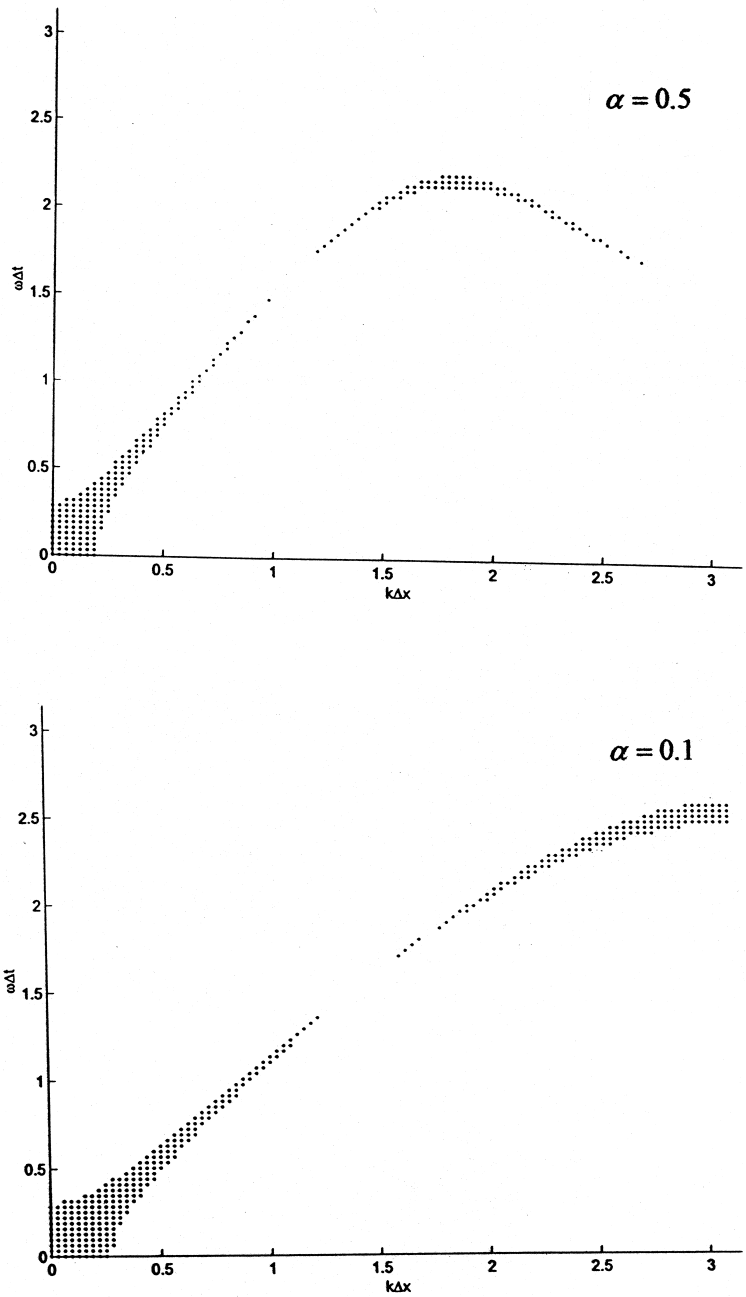

Figure 4. The DRP region in non-dimensional wave number-frequency for the slope limiter scheme [6] for the same values of α shown in Figure 3.

Similarly one can obtain the pair of amplification factors from the quadratic equation

$$G^2 + aG - b = 0 \tag{16}$$

where

$$b = N_C\{\sin^2(k\Delta x/2)[1 - \varepsilon(\kappa \sin^2(k\Delta x/2)) - \cos^2(k\Delta x/2)] + \frac{i}{2}\sin(k\Delta x)[1 + \varepsilon(1-\kappa)\sin^2(k\Delta x/2)]\}$$

$$a = -1 + 3b$$

One can obtain the numerical group velocity by differentiating Equation (15) and simplifying, to get

$$V_{gn} = \frac{i\dfrac{db}{dk} - \dfrac{da}{dk}\sin(\omega\Delta t)}{\Delta t[2\cos(2\omega\Delta t) + a\cos(\omega\Delta t)]} \tag{17}$$

In Figure 5, G_1 and G_2 the two roots of the quadratic gives by Equation (16), are shown for $N_C = 0.1$ for the FVS schemes given by Equation (7). Note that G_1 is the severely attenuated factor while G_2 resembles the amplification factors of the Euler time marching schemes shown in Figure 1, except for the central difference scheme of second order. While for the Euler time marching scheme, a second-order central difference scheme was found to be unconditionally unstable, here it is conditionally stable, i.e. it is stable for the low values $k\Delta x$. Once again, the one-sided linear interpolation scheme, the first-order upwinding scheme and the linear interpolation schemes are excessively dissipative and cannot be used for high Reynolds number applications until and unless a very refined mesh is used. Also, between MUSCL and QUICK schemes, the latter is less dissipative and hence should be favored. It is seen that as CFL numbers are reduced, all the schemes show stability with amplification factors approaching neutral stability—a desired property. Overall this time integration scheme is overtly dissipative because of the presence of G_1 and hence should not be used for high accuracy calculations. Because of the serious attenuation exhibited by the amplification factor $G_{1,}$ that would preclude the usage of this time integration scheme, the DRP region of these combined schemes are not pursued. However, it is interesting to note that some researchers in their so-called DNS work have used the Adams–Bashforth time integration. For example, Kim and Moin [8] have used CD_2 spatial discretization and the Adams–Bashforth time integration scheme in their DNS studies of channel flow. Figure 5 shows that G_2 has the interesting property of near neutral behavior at the smallest and Nyquist limit. In many fluid dynamic systems the small scale disturbances like free stream turbulence drives the transition to turbulence and thus the present scheme would appear to be natural as far as this component of the amplification factor is concerned. But it is the presence of G_1 which is so attenuating that the Adams–Bashforth scheme will be totally inadequate for DNS studies and hence would not be discussed with respect to its DRP property.

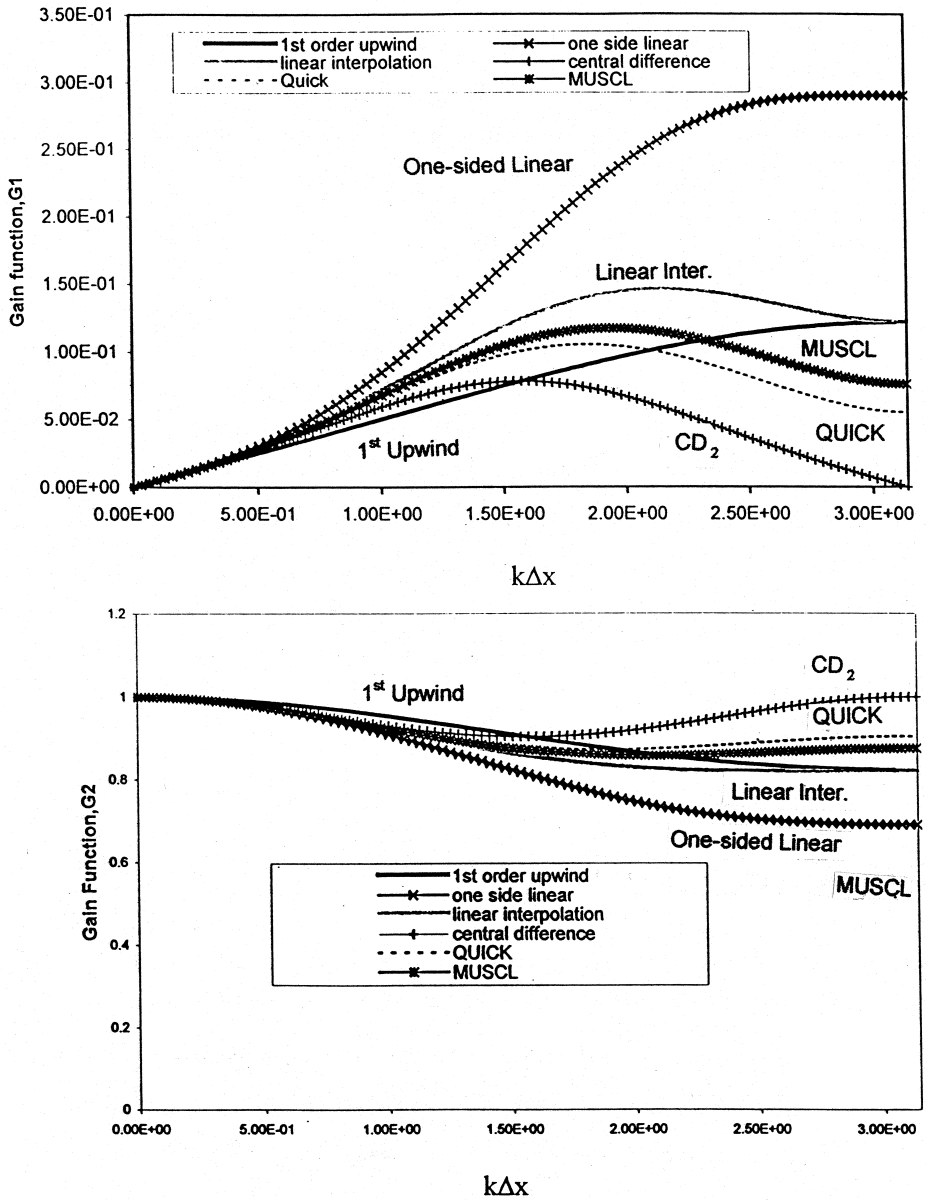

Figure 5. The amplification factor (G) for (ε–κ) FVS-FV schemes for which time integration is performed by an Adams–Bashforth scheme plotted against non-dimensional wave number. Shown on top is the severely attenuated root and the near neutral root is shown below.

Next, some of the multi-time step integration schemes are investigated. These are the TVD Runge–Kutta schemes for temporal discretization as given in [9]. For the two-stage Runge–Kutta time integration scheme given for the equation

$$\frac{\partial u}{\partial t} = L(u) \tag{18a}$$

by

$$\begin{aligned} U^{(1)} &= U^n + \Delta t L(U^n) \\ U^{n+1} &= \frac{U^n + U^{(1)}}{2} + \frac{\Delta t}{2} L(U^{(1)}) \end{aligned} \tag{18b}$$

For this scheme applied to Equation (1) gives the amplification factor as

$$G_{\mathrm{RK}_2} = 1 - N_{\mathrm{C}} g + \frac{N_{\mathrm{C}}^2}{2} g^2 \tag{19}$$

where

$$\begin{aligned} g = a + \mathrm{i}b = 2\sin^2\frac{k\Delta x}{2} + \frac{\varepsilon(1-\kappa)}{2}\cos(k\Delta x)(\cos(k\Delta x) - 1) - \varepsilon(1-\kappa)\sin^2\frac{k\Delta x}{2} \\ + \mathrm{i}\sin(k\Delta x)\left[1 + \frac{\varepsilon(1-\kappa)}{2}(1 - \cos(k\Delta x))\right] \end{aligned}$$

The numerical group velocity is given by

$$V_{\mathrm{gn}} = \frac{c}{\Delta x \cos(\omega \Delta t)}\left[\frac{\mathrm{d}b}{\mathrm{d}k} - N_{\mathrm{C}}\left(b\frac{\mathrm{d}a}{\mathrm{d}k} + a\frac{\mathrm{d}b}{\mathrm{d}k}\right)\right]$$

In Figure 6 the amplification factors—for all the six schemes given by Equation (7)—are plotted for three CFL numbers (= 0.01, 0.2 and 0.5). For the RK_2 time integration scheme, the OSL interpolation is not only excessively dissipative, but when the CFL number is increased from 0.2 to 0.5, the phase error is so large that for a physical system for which the wave propagates downstream, the numerical scheme would predict a disturbance field whose wave numbers components given by $k\Delta x \geq 1.57$ would travel upstream. The other interpolation schemes are such that the intermediate wave numbers are the most damped and for the first-order upwinding it is the lowest and highest wave numbers that are least damped and in that sense it is an interesting scheme. Between the two higher-order schemes, the QUICK scheme is the least dissipative scheme.

In Figure 7(a)–(d) the DRP region of some of the schemes are displayed for the RK_2 time integration scheme. In Figure 7(a) the second-order central difference scheme result is shown and it is interesting to note that the DRP region does not depend on the CFL number because

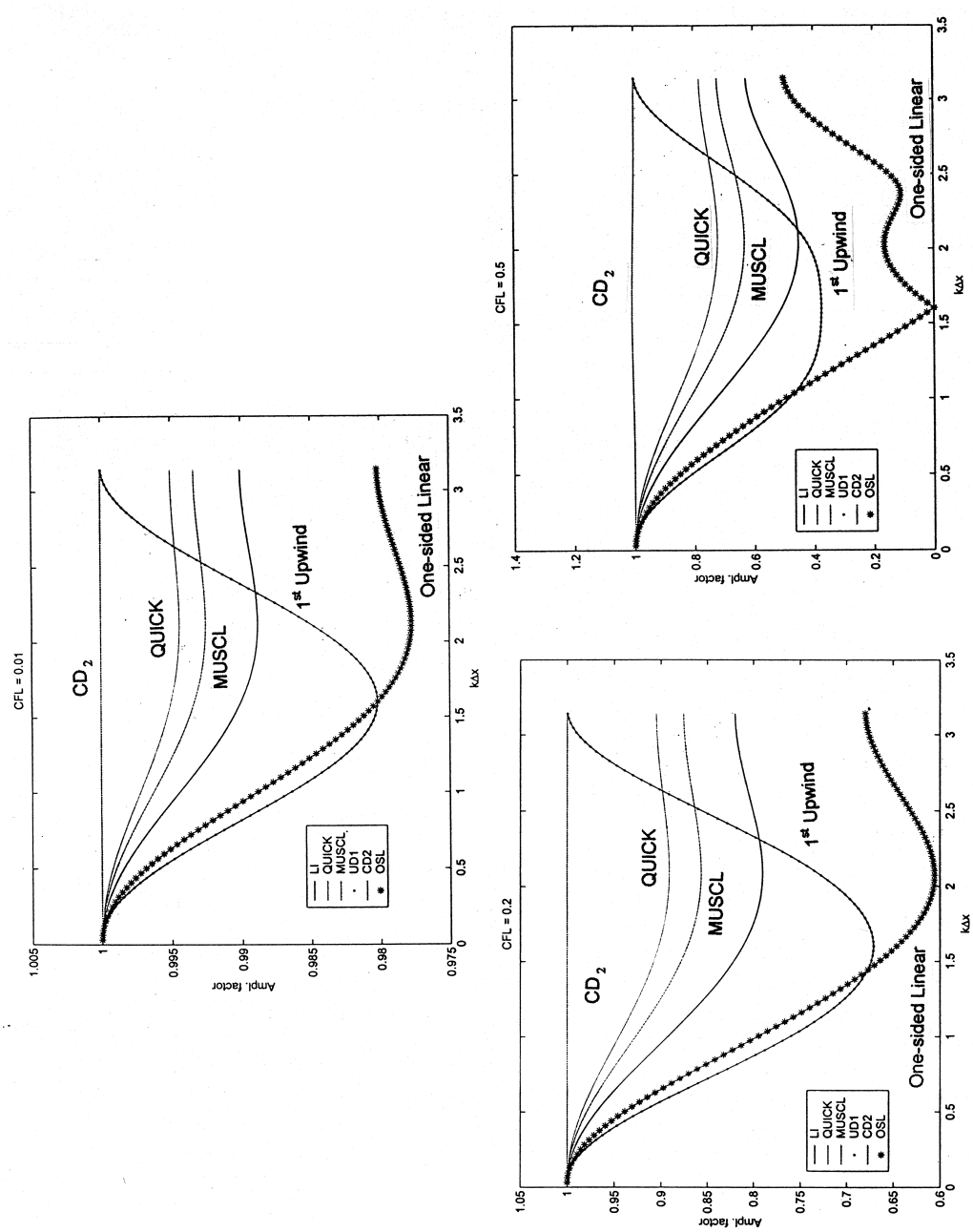

Figure 6. The amplification factor (G) for (ε–κ) FVS-FV schemes for which time integration is performed by a two-stage Runge–Kutta scheme plotted against non-dimensional wave number for three different CFL numbers.

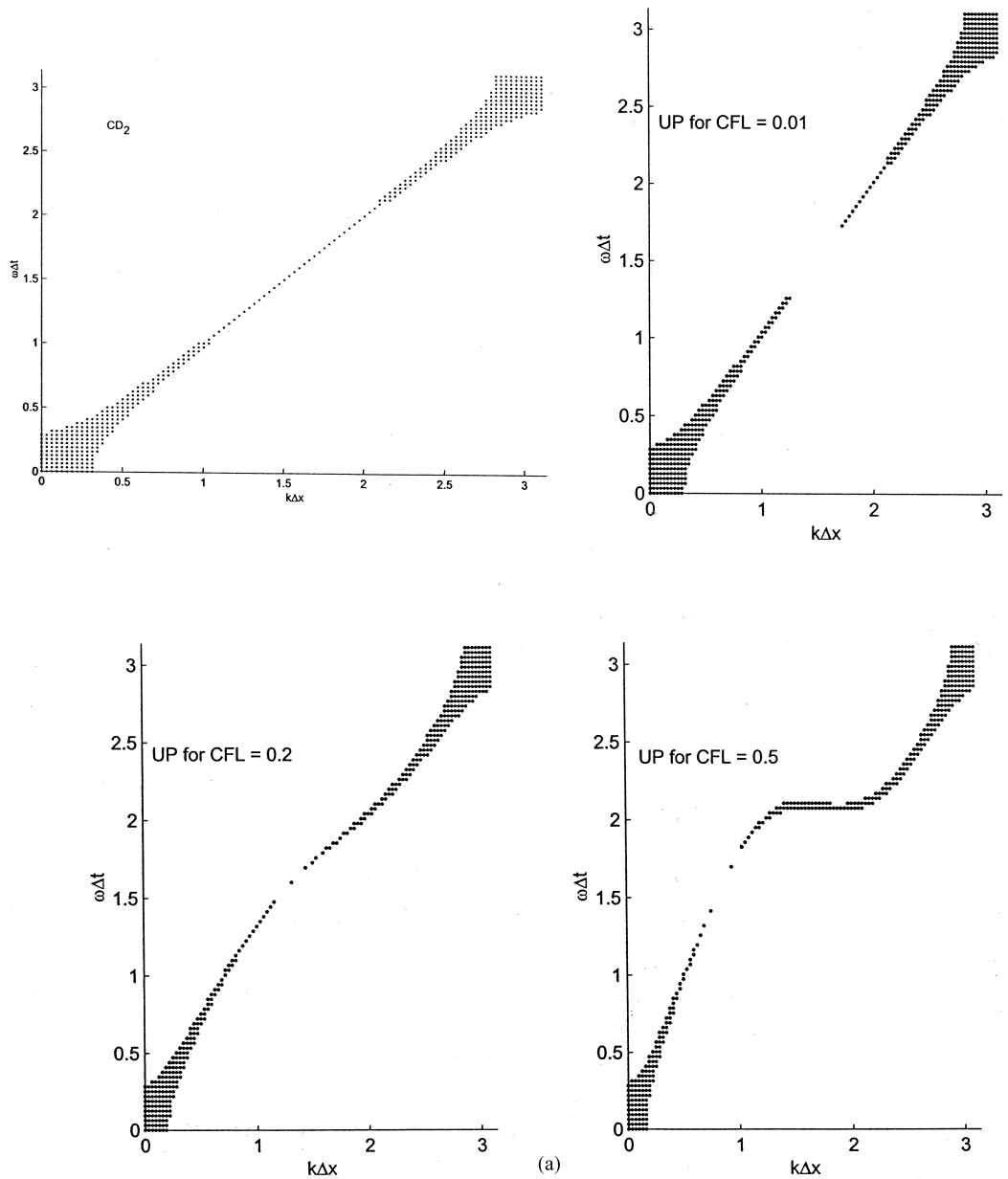

Figure 7. (a) The DRP region of the RK_2 scheme for CD_2 and first-order upwind spatial discretization schemes. Note that the CD_2 results do not depend on CFL number. (b) The DRP region of the RK_2 scheme for the LI spatial discretization scheme for different CFL numbers. (c) The DRP region of the RK_2 scheme for QUICK spatial discretization schemes. (d) The DRP region of the RK_2 scheme for the MUSCL spatial discretization scheme.

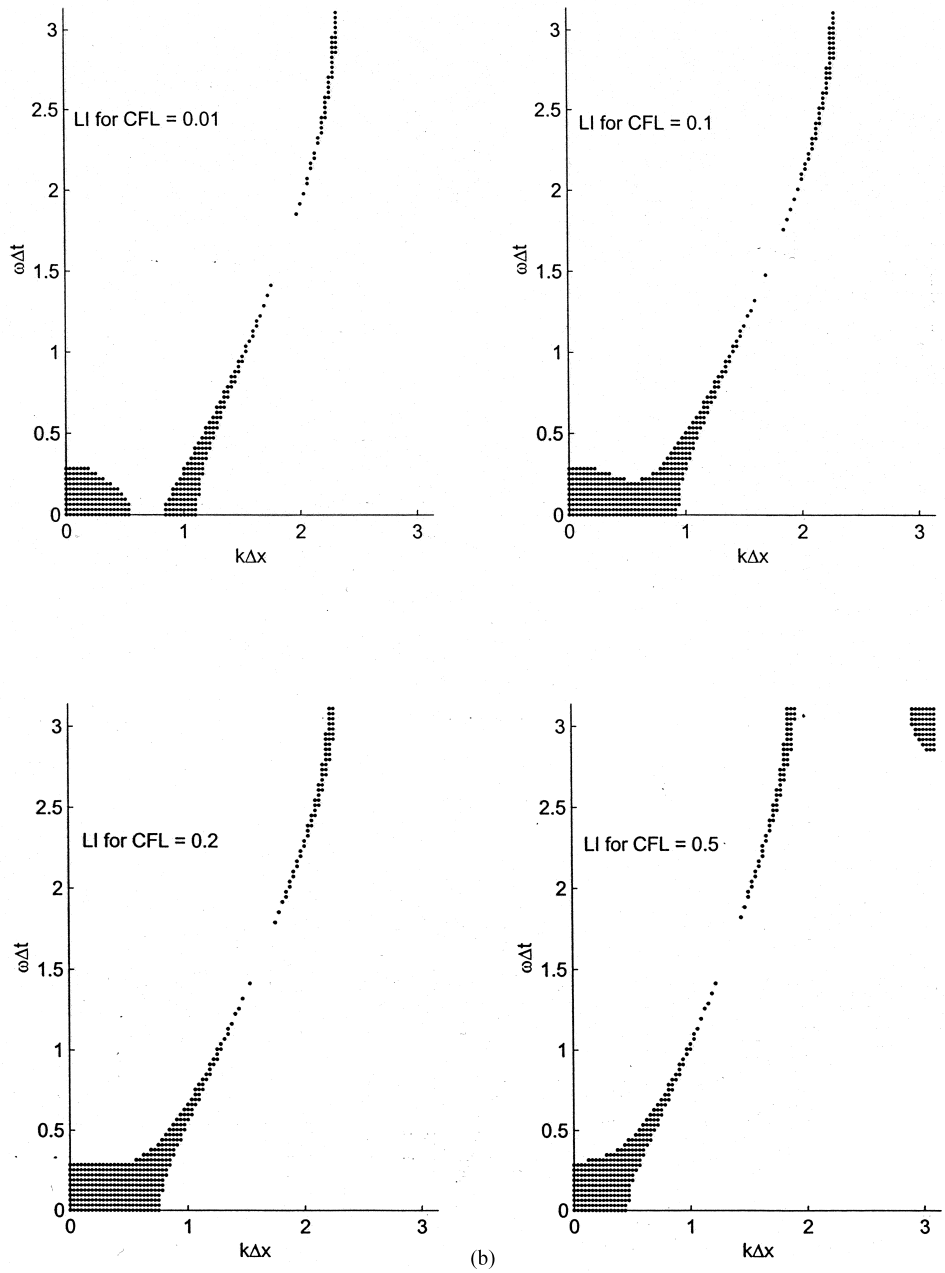

(b)

Figure 7 (*Continued*)

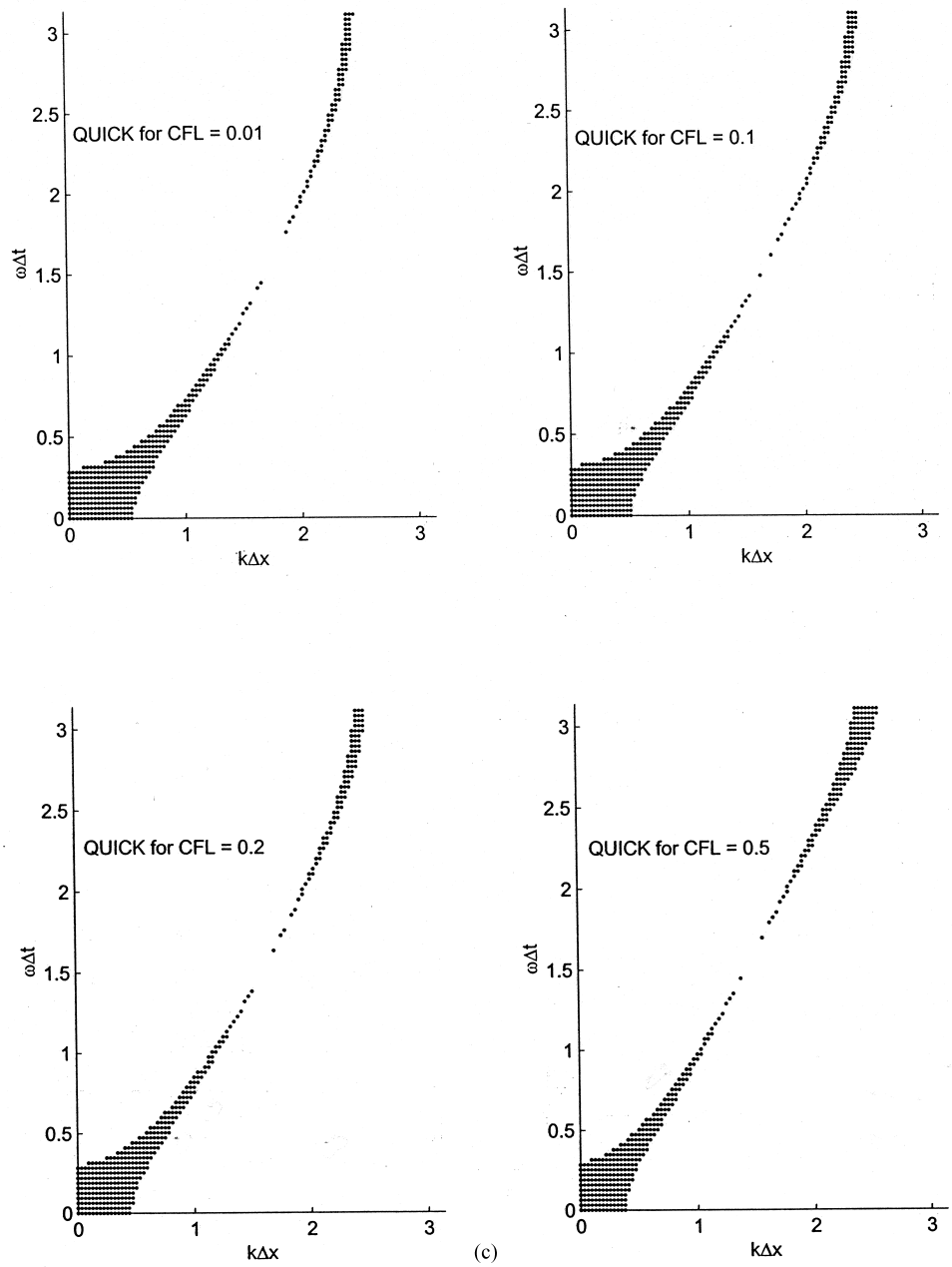

Figure 7 (*Continued*)

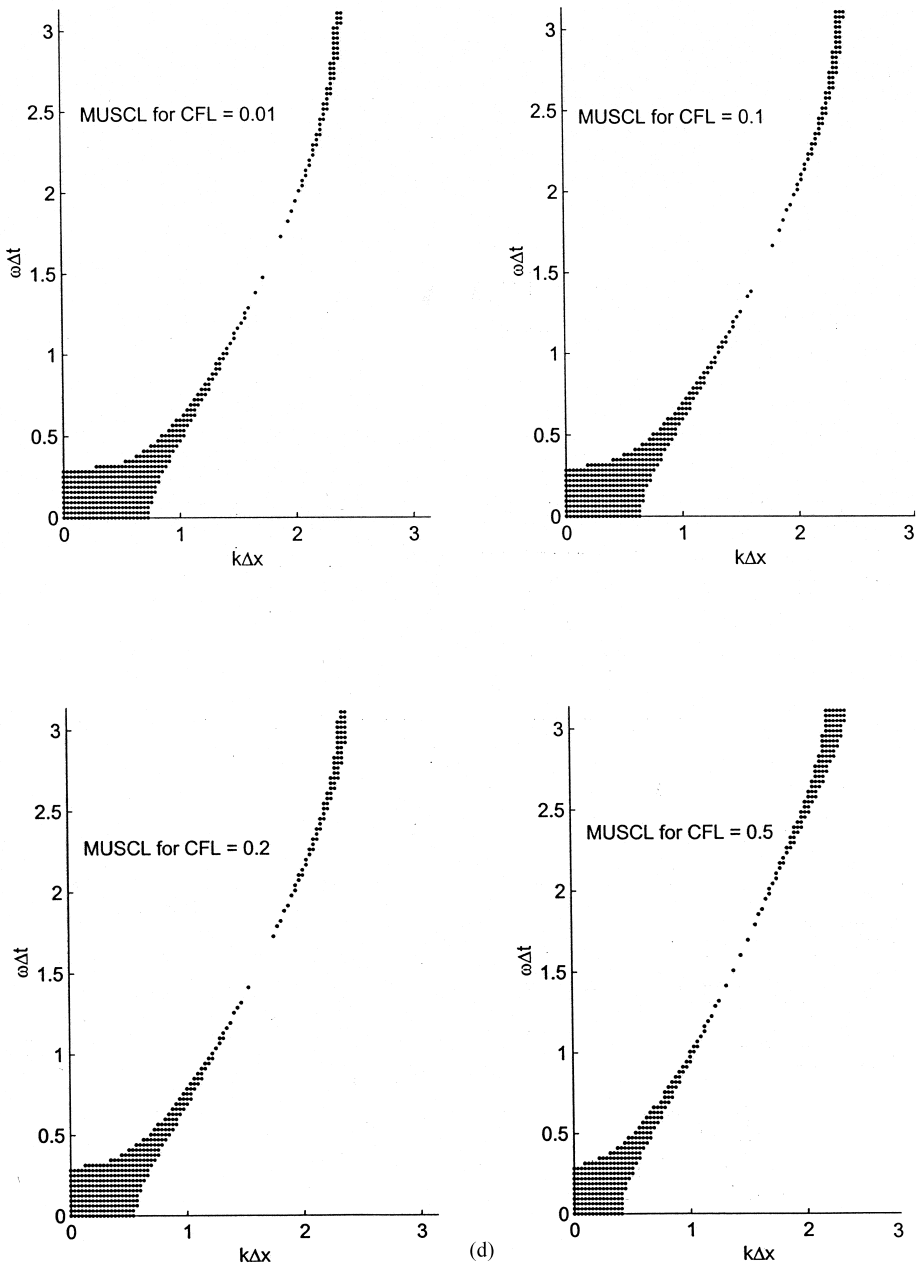

(d)

Figure 7 (*Continued*)

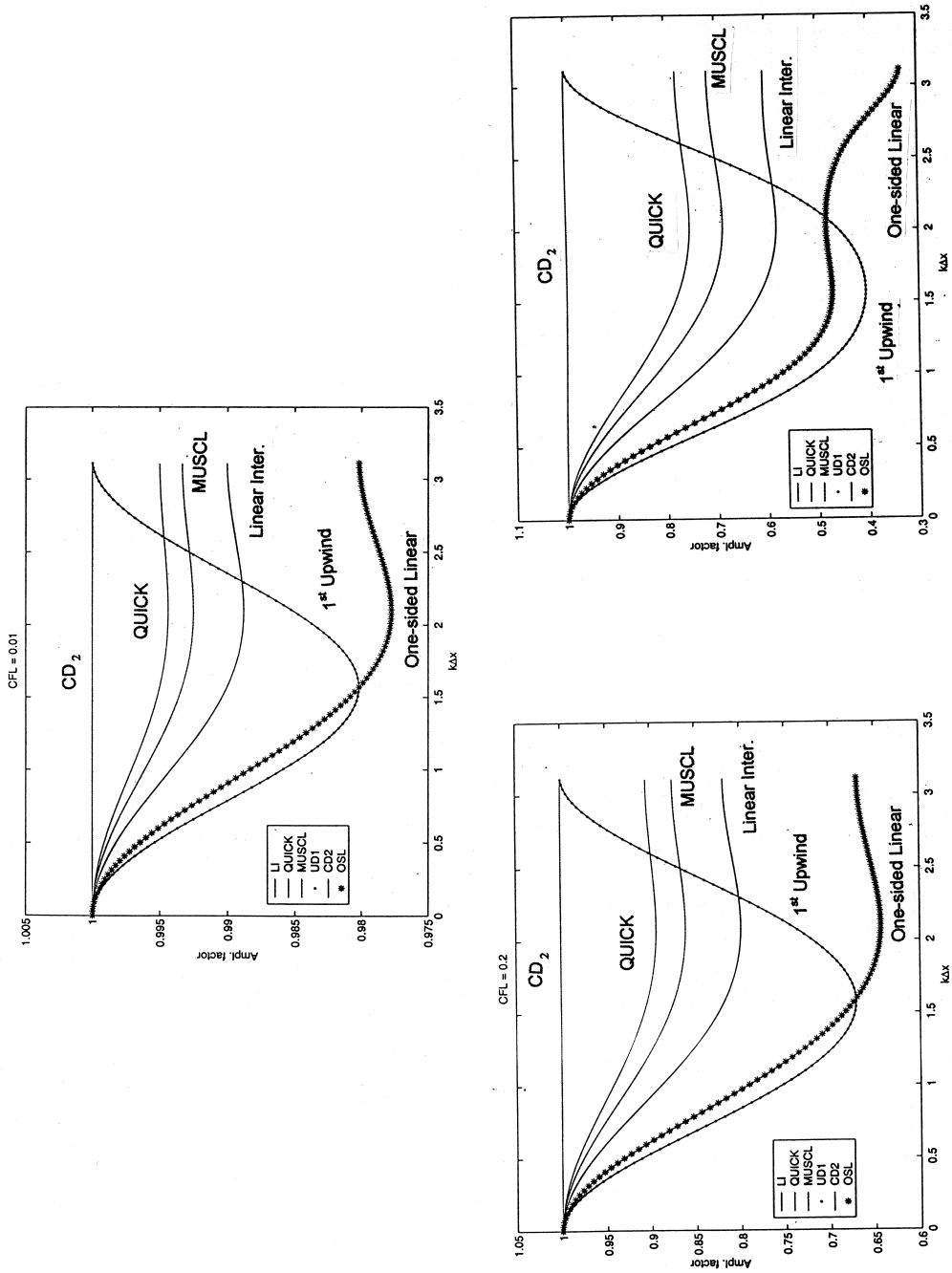

Figure 8. The amplification factor (G) for (ε–κ) FVS-FV schemes for which time integration is performed by a three-stage Runge–Kutta scheme plotted against non-dimensional wave number for three different CFL numbers.

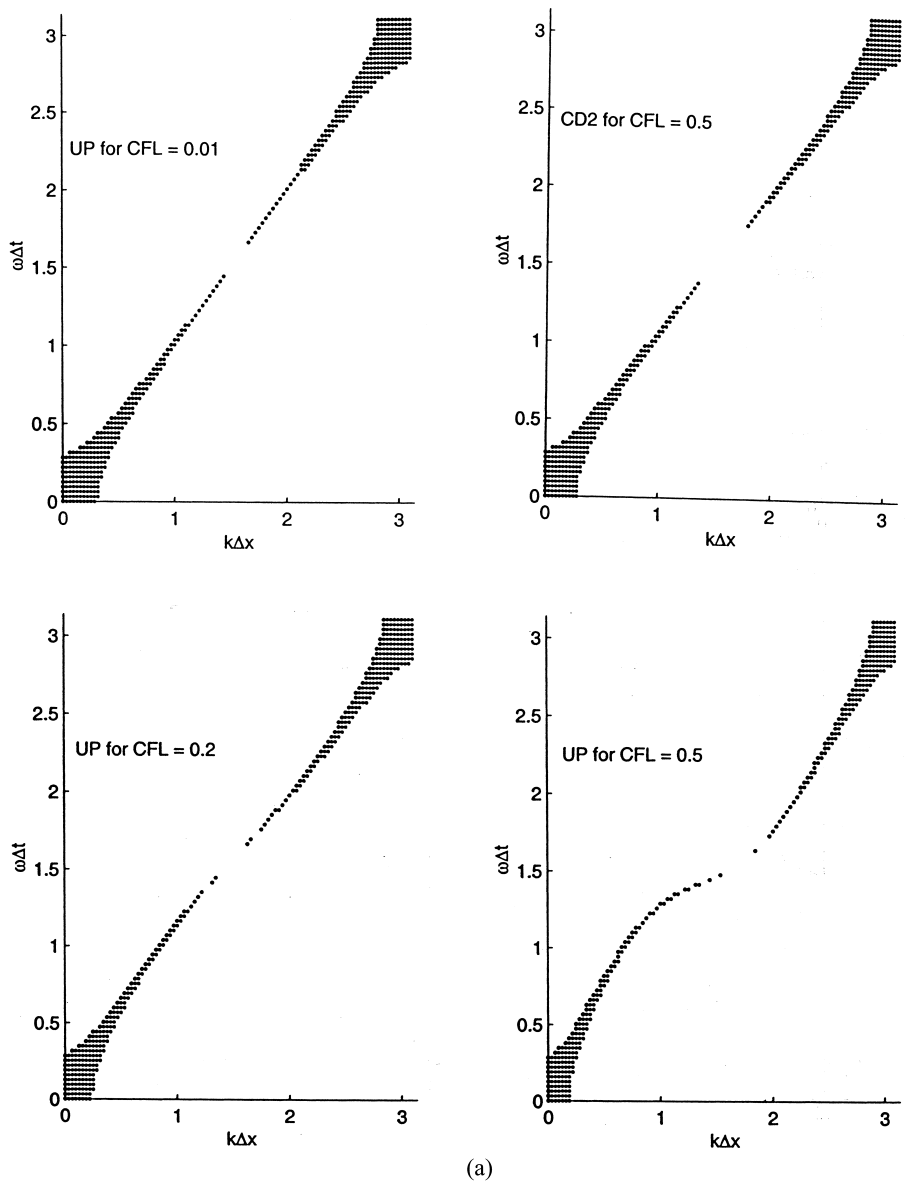

(a)

Figure 9. (a) The DRP regions of the RK_3 scheme for CD_2 and first-order upwind spatial discretization schemes. Note that the CD_2 results fo not depend on CFL number. (b) The DRP region of the RK_3 scheme for the LI spatial discretization scheme for different CFL numbers. (c) The DRP region of the RK_3 scheme for the QUICK spatial discretization schemes for indicated CFL numbers. (d) The DRP region of the RK_3 scheme for the MUSCL spatial discretization scheme for indicated CFL numbers.

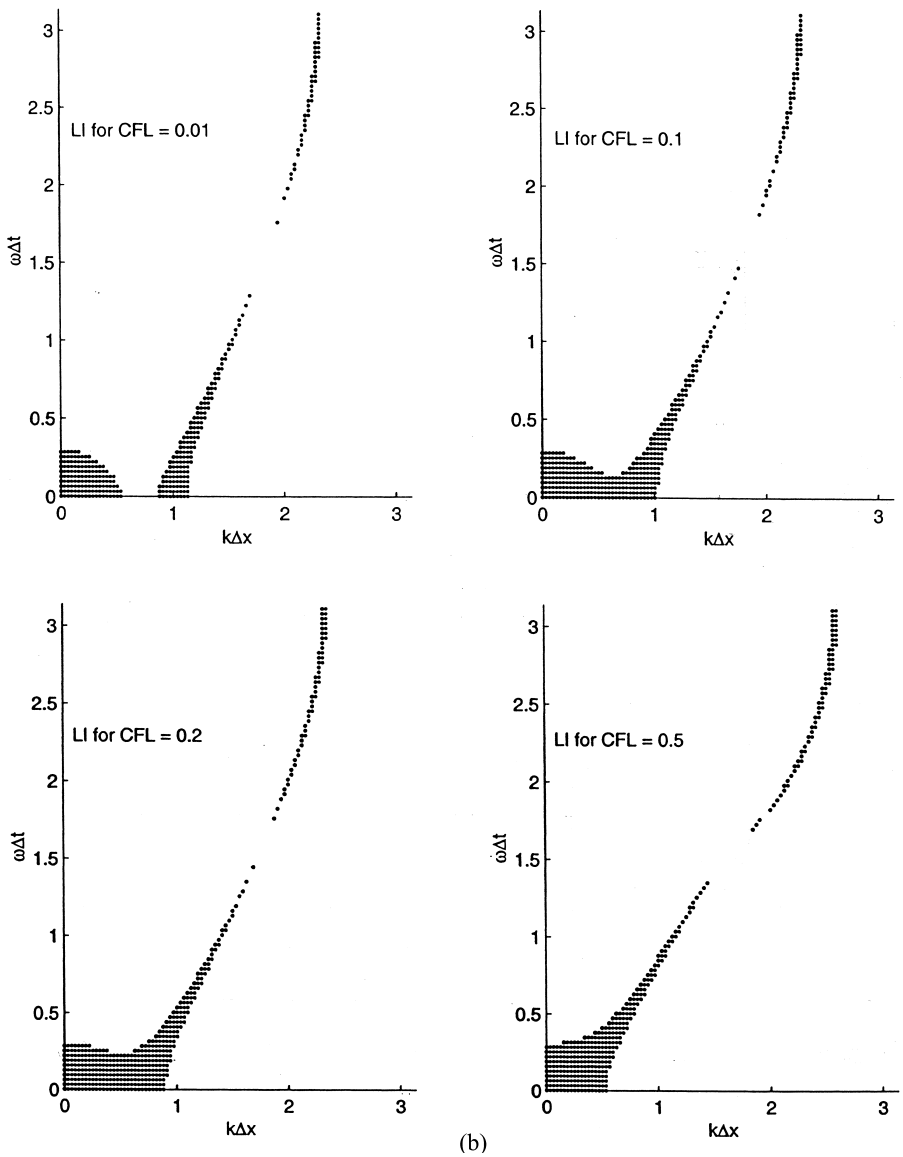

(b)

Figure 9 (*Continued*)

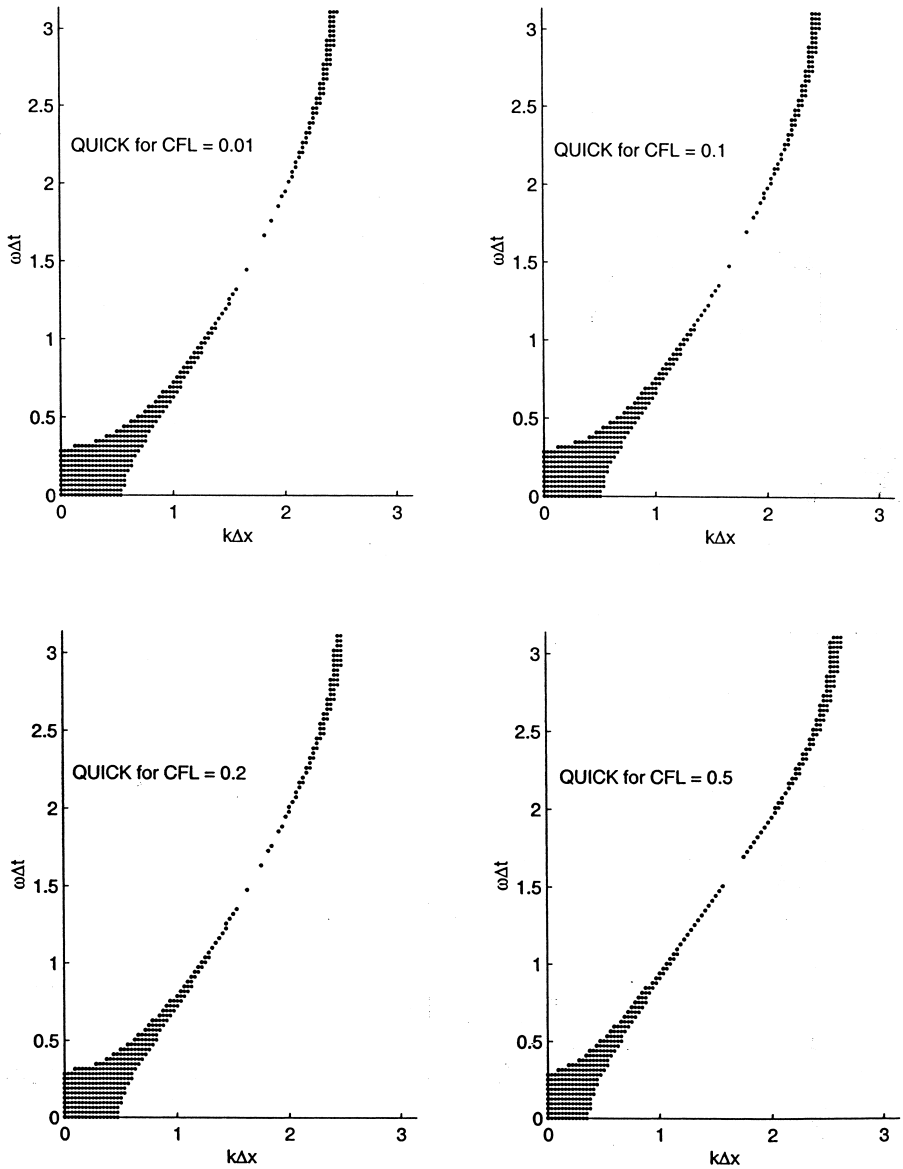

(c)

Figure 9 (*Continued*)

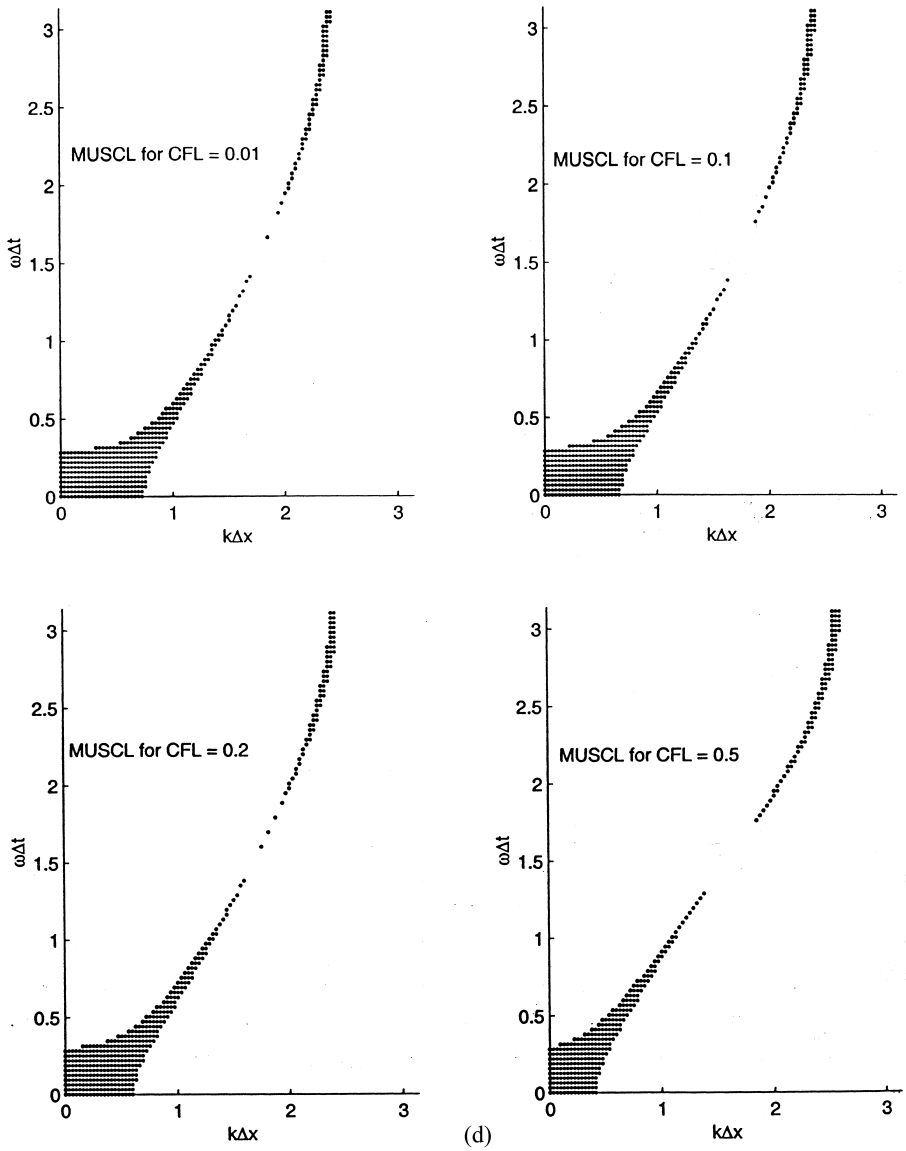

(d)

Figure 9 (*Continued*)

in Equatuion (20) $\mathrm{d}a/\mathrm{d}k$ and $\mathrm{d}b/\mathrm{d}k$ are both zero for the combination of ε and κ. Once numerical stability is ensured, one can use the CD_2 scheme while the DRP property is being preserved when the CFL number is increased to any value. This is a feature that is not shared by any other space-time integration schemes. This is a positive attribute of the scheme and would be useful for high Reynolds number flow simulation. Comparatively the first-order upwind scheme results shown in Figure 7(b) shows that the $k\Delta x$ range over which the DRP property is valid keeps reducing, while the $\omega\Delta t$ range does not change with CFL number. For lower CFL numbers the first-order upwind scheme performance is identical to second-order central difference scheme. In Figure 7(c) and (d) the QUICK and MUSCL schemes DRP region is shown and for these schemes the $\omega\Delta t$ range also does not change with CFL number and this is same for both the schemes. But the wave number range is a strong function of CFL number and for lower CFL numbers the MUSCL scheme has a better range of $k\Delta x$ over which the dispersion relation is preserved. However, at higher CFL numbers (larger than 0.2) the $k\Delta x$ range for both methods are the same.

Similarly, for Equation (18a), the three-stage Runge–Kutta scheme is given by

$$\begin{aligned} U^{(1)} &= U^n + \Delta t L(U^n) \\ U^{(2)} &= \frac{3}{4} U^n + \frac{U^{(1)}}{4} + \frac{\Delta t}{4} L(U^{(1)}) \\ U^{n+1} &= \frac{U^n}{3} + \frac{2}{3} U^{(2)} + \frac{2}{3} \Delta t L(U^{(2)}) \end{aligned} \tag{21}$$

And for this time integration scheme with the space discretization scheme given by Equation (7), the amplification rate is given by

$$G_{\mathrm{RK}_3} = 1 - N_{\mathrm{C}} g + \frac{N_{\mathrm{C}}^2 g^2}{2} - \frac{N_{\mathrm{C}}^3 g^3}{6} \tag{22}$$

And the numerical group velocity is given by

$$V_{\mathrm{gn}} = \frac{c}{\cos(\omega\Delta t)} \left[\frac{\mathrm{d}b}{\mathrm{d}k} - \frac{N_{\mathrm{C}}}{2} \left(a \frac{\mathrm{d}b}{\mathrm{d}k} + b \frac{da}{dk} \right) + \frac{N_C^2}{6} \left(4ab \frac{\mathrm{d}a}{\mathrm{d}k} - 3b^2 \frac{\mathrm{d}b}{\mathrm{d}k} \right) \right] \tag{23}$$

These types of time integration schemes have been used for both incompressible and compressible flows (shock-capturing TVD scheme) by Le and Moin [10] and Shu and Osher [11,12] respectively.

In Figure 8 the amplification rates for all six discretization schemes are shown for different values of CFL numbers. While the trends and values are similar at smaller CFL numbers, it is the OSL scheme that shows different behavior for a CFL number of 0.5 when the results are compared with the RK_2 scheme. The DRP regions for different spatial discretization schemes for RK_3 time integration schemes are shown in Figure 9(a) and (b). Once again the DRP region for the CD_2 scheme does not depend on the CFL number and the region is indistinguishable from the RK_2 results. The first-order upwind scheme results also behave similarly. Once again the LI scheme shows extended wave number range over which the DRP property is valid in the

intermediate values of the CFL number. Even for very high CFL numbers the DRP region is larger as compared to the CD_2 scheme results.

Also, the higher-order interpolation schemes (QUICK and MUSCL) do not show any appreciable change of the DRP region. This thus shows that there are hardly any additional benefits in choosing the three-stage Runge–Kutta time integration scheme over the two-stage Runge–Kutta time integration. It is the simplicity and lesser storage requirement of the latter over the former, which should decide in favor of the RK_2 scheme.

ACKNOWLEDGMENTS

The first author wishes to acknowledge the help provided by Mr Manojit Chatopadhyay and Mr Kabit Mohammad of NUS, Singapore, in preparing some of the figures.

REFERENCES

1. Sengupta TK, Sengupta R. Flow past an impulsively started circular cylinder at high Reynolds number. *Computational Mechanics* 1994; **14**(4): 298–310.
2. Sengupta TK, Gupta K. Tailoring higher order methods for DNS and LES. In *Proceedings of the 3rd Asian CFD Conference*, Prahlad TS, Deshpande SM, Saxena SK (eds). Graphic Arts Div. of NAL Bangalore: Bangalore, India, 1998; 94–97.
3. Sengupta TK, Nair MT. Upwind schemes and large eddy simulation. *International Journal for Numerical Methods in Fluids* 1999; **31**: 879–889.
4. Kravchenko AG, Moin P. On the effects of numerical errors in large eddy simulations of turbulent flows. *Journal of Computational Physics* 1997; **131**: 310–322.
5. Bhandari GH. Navier–Stokes solver using higher order interpolation for compressible flow past cascades. MTech thesis, Department of Aerospace Engineering, IIT, Kanpur, 1998.
6. Causon DM, Ingram DM, Yang G. On application of high resolution shock capturing methods to unsteady flows. In *Numerical Methods for Wave Propagation*, Toro EF, Clarke JF (eds). Kluwer: Netherlands, 1998; 145–171.
7. Hirsch C. *Numerical Computation of Internal and External Flows*, vol. 2. Wiley: Guildford, UK, 1985.
8. Kim J, Moin P. Application of a fractional step method to incompressible Navier–Stokes equation. *Journal of Computational Physics* 1985; **58**: 308–322.
9. Gottlieb S, Shu C-W. Total variation diminishing Runge–Kutta schemes. NASA ICASE Report No. 96-50, 1996.
10. Le H, Moin P. An improvement of fractional stem methods for the incompressible Navier–Stokes equation. *Journla of Computational Physics* 1991; **92**: 369–379.
11. Shu C-W, Osher S. Efficient implementation of essentially non-oscillatory shock capturing schemes. *Journla of Computational Physics* 1988; **77**: 439–471.
12. Shu C-W, Osher S. Efficient implementation of essentially non-oscillatory shock capturing schemes—II. *Journal of Computational Physics* 1989; **83**: 32–78.

